Even- and odd-order dispersion cancellation effects in four-photon quantum interferometry

Jing Qiu (邱 婧)[1], Guoyong Xiang (项国勇)[2], Yongsheng Zhang (张永生)[2], Shensheng Han (韩申生)[1], and Youzhen Gui (桂有珍)[1*]

[1]*Shanghai Institute of Optics and Fine Mechanics, Chinese Academy of Sciences, Shanghai 201800, China*

[2]*Laboratory of Quantum Information, University of Science and Technology of China, Hefei 230026, China*

[*]*Corresponding author: yzgui@siom.ac.cn*

Received April 16, 2014; accepted September 11, 2014; posted online October 27, 2014

The even-order dispersion cancellation effect based on the frequency anti-correlated photon pairs has attracted much attention in the research of quantum dispersion cancellation in two-photon systems. In this letter, we demonstrate a four-photon quantum interferometry in which we can not only observe the even-order dispersion cancellation effect but also the odd-order cancellation. Importantly, the four-photon scheme can get a much better resolution than the two-photon case and help us get a better understanding of the interference phenomenon in a four-photon interferometry.

OCIS codes: 270.1670, 270.5290, 270.5570.
doi: 10.3788/COL201412.112701.

If a beam of light, especially ultrafast pulses with large bandwidth, propagates through a dispersive medium, the temporal file gets broadened and thus can have a detrimental effect on the timing information in which we are interested. In this case, dispersion cancellation has always been a venerable problem in both classical and quantum fields such as clock synchronization[1–3] and optical coherence tomography[4,5].

In quantum optics, there are mainly two types of dispersion cancellation scenarios which are based on the entangled photons produced by the process of spontaneous parametric down-conversion (SPDC)[6]. The first one showed that even with only one dispersive medium in one arm of the Hong-Ou-Mandel (HOM) interferometer, the resolution of the time interval between photons was not significantly degraded due to the frequency anti-correlation of the conjugate photons[7,8]. The other one proposed by Franson[9,10] showed a nonlocal effect that if a pair of energy–time entangled photons propagated through two distant dispersive media with equal dispersion coefficients but opposite in sign, the dispersion effect occurred in one medium can be cancelled out by the dispersion in the other one.

In subsequent experimental works, these two kinds of dispersion cancellation effects have been proved[11–14]. These are the well-known even-order dispersion cancellation effects. In 2009, Minaeva *et al.* showed an interesting effect that both the even- and odd-order dispersion cancellation effects can be observed in a single quantum interferometer by using frequency anti-correlated photon pairs[15].

With the interesting and significant phenomena shown in the two-photon system, multi-photon system also displays its fascinating results to researchers and many groups make great efforts to study the multi-photon state, for example, the preparation of the multi-photon state[16–18] and the quantum effects shown in the multi-photon system[19,20]. Compared with the two-photon system, multi-photon entangled state has more advantages in the fields of quantum information and quantum computation. It has been shown that multi-photon system can greatly improve the accuracy of precision phase measurement, reaching the Heisenberg limit[21–27]. In this letter, we report a theoretical dispersion cancellation scheme based on a four-photon source from which we can get a better resolution than the two-photon project. More interestingly, both the even- and odd-order dispersion cancellation effects can be observed in this interferometer.

Our scheme is illustrated in Fig. 1. Four-photon generated from the SPDC process are sent into a HOM interferometer. Each output of the HOM interferometer, named C and D, provides inputs to a Mach–Zehnder (MZ) interferometer, respectively. Two photons as a whole get into the upper MZ interferometer, whereas the other two as a whole get into the lower one. The time delay τ_1 in the signal arm of the HOM interferometer can be tuned continuously so that we can control the state of light led into the MZ interferometer. In each MZ interferometer, there is a strong dispersive medium which provides a phase shift ϕ and a fixed time delay τ_2 in the upper arm. When we get coincidence count rates from the four detectors[28,29], a special interference pattern occurs (Fig. 2).

Firstly, we assume that the four photons are produced in the form that two identical pairs of frequency anti-correlated bi-photon generated simultaneously from the SPDC process with high-power continuous pump laser. In that case the four-photon frequency-entangled states arriving at the last beam splitter (BS) of the HOM interferometer can be presented as

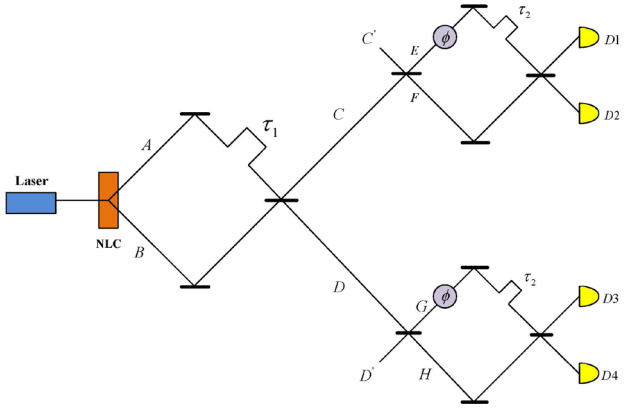

Fig. 1. Outline of the four-photon quantum interferometry. Four-photons generated from the process of SPDC split into two pairs on the output side of the BS in the HOM interferometer. The signal arm can be scanned by modulating the tunable time delay τ_1. Each pair is sent into a MZ interferometer. In each MZ interferometer, there is a dispersive medium and a fixed time delay in one arm. Coincidence count rates can be measured by four detectors, D1, D2, D3, and D4.

$$\left|\varphi\right\rangle = \int \mathrm{d}\omega_{\mathrm{A}}\mathrm{d}\omega_{\mathrm{B}}\mathrm{d}\omega_{\mathrm{A}}^{'}\mathrm{d}\omega_{\mathrm{B}}^{'}\Phi(\omega_{\mathrm{A}},\omega_{\mathrm{B}})\Phi(\omega_{\mathrm{A}}^{'},\omega_{\mathrm{B}}^{'})\hat{a}_{\mathrm{A}}^{\dagger}\left(\omega_{\mathrm{A}}\right)\hat{a}_{\mathrm{A}}^{\dagger}\left(\omega_{\mathrm{A}}^{'}\right)\hat{a}_{\mathrm{B}}^{\dagger}\left(\omega_{\mathrm{B}}\right)\hat{a}_{\mathrm{B}}^{\dagger}\left(\omega_{\mathrm{B}}^{'}\right)\exp\left[-\mathrm{i}\left(\omega_{\mathrm{A}}+\omega_{\mathrm{A}}^{'}\right)\tau_1\right]\left|0\right\rangle, \quad (1)$$

where $\Phi\left(\omega_{\mathrm{A}},\omega_{\mathrm{B}}\right)$ is determined by the phase matching function with $\Phi\left(\omega_{\mathrm{A}},\omega_{\mathrm{B}}\right)=\Phi\left(L\Delta\mathrm{k}\right)\Big|_{\omega_{\mathrm{p}}=\omega_{\mathrm{A}}+\omega_{\mathrm{B}}}$, L is the length of the crystal, and $\Delta k = k_{\mathrm{p}}\left(\omega_{\mathrm{p}}\right)-k_{\mathrm{A}}\left(\omega_{\mathrm{A}}\right)-k_{\mathrm{B}}\left(\omega_{\mathrm{B}}\right)$ is the phase mismatch quantity.

The positive electrical field operators at detectors, D1, D2, D3, and D4 are defined by

$$\hat{E}_1^{(+)}\left(t_1\right)=\int \mathrm{d}\omega_1\hat{a}_1\left(\omega_1\right)\exp\left(-\mathrm{i}\omega_1 t_1\right),$$

$$\hat{E}_2^{(+)}\left(t_2\right)=\int \mathrm{d}\omega_2\hat{a}_2\left(\omega_2\right)\exp\left(-\mathrm{i}\omega_2 t_2\right),$$

$$\hat{E}_3^{(+)}\left(t_3\right)=\int \mathrm{d}\omega_3\hat{a}_3\left(\omega_3\right)\exp\left(-\mathrm{i}\omega_3 t_3\right),$$

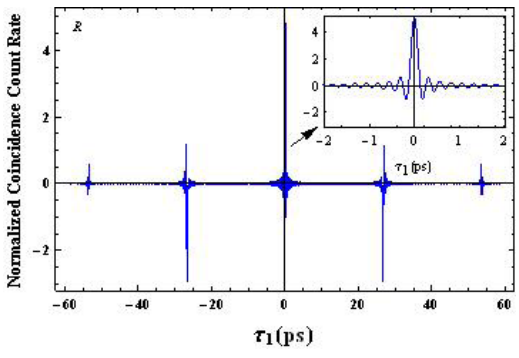

Fig. 2. Coincidence count rate of the four detectors. There are mainly five interference fringes emerging when we scan the tunable time delay τ_1. A central peak is shown in the middle region of $\tau_1 \approx 0$ ps, with four side fringes shown in the region of $\tau_1 \approx \pm 26$ and ± 52 ps .

$$\hat{E}_4^{(+)}\left(t_4\right)=\int \mathrm{d}\omega_4\hat{a}_4\left(\omega_4\right)\exp\left(-\mathrm{i}\omega_4 t_4\right), \quad (2)$$

where $\hat{a}_j\left(\omega_j\right)$ $(j=1, 2, 3, 4)$ is the annihilation operator in each detector field. The relations between the annihilation operators in the output and the input ports of the MZ interferometer are

$$\begin{pmatrix}\hat{a}_1\left(\omega\right)\\ \hat{a}_2\left(\omega\right)\end{pmatrix}=\begin{pmatrix}a\left(\omega\right) & \beta\left(\omega\right)\\ \beta\left(\omega\right) & a\left(\omega\right)\end{pmatrix}\begin{pmatrix}\hat{a}_{C'}\left(\omega\right)\\ \hat{a}_C\left(\omega\right)\end{pmatrix},$$

$$\begin{pmatrix}\hat{a}_3\left(\omega\right)\\ \hat{a}_4\left(\omega\right)\end{pmatrix}=\begin{pmatrix}a\left(\omega\right) & \beta\left(\omega\right)\\ \beta\left(\omega\right) & a\left(\omega\right)\end{pmatrix}\begin{pmatrix}\hat{a}_D\left(\omega\right)\\ \hat{a}_{D'}\left(\omega\right)\end{pmatrix}, \quad (3)$$

where C and C' denote the two input ports of the upper MZ interferometer, and D and D' denote the lower one. The terms $\alpha(\omega)$ and $\beta(\omega)$ are presented in the form of

$$a\left(\omega\right)=\frac{1}{2}\left\{\exp\left[\mathrm{i}\frac{\omega\tau_2+\varphi\left(\omega\right)}{2}\right]+\exp\left[-\mathrm{i}\frac{\omega\tau_2+\varphi\left(\omega\right)}{2}\right]\right\},$$

$$\beta\left(\omega\right)=\frac{1}{2}\left\{\exp\left[\mathrm{i}\frac{\omega\tau_2+\varphi\left(\omega\right)}{2}\right]-\exp\left[-\mathrm{i}\frac{\omega\tau_2+\varphi\left(\omega\right)}{2}\right]\right\}. \quad (4)$$

For simplicity, we use terms cos[Θ(ω)] and sin[Θ(ω)] instead of $\alpha(\omega)$ and $\beta(\omega)$.

$$\cos\left[\Theta\left(\omega\right)\right]=a\left(\omega\right)=\frac{1}{2}\left\{\exp\left[\mathrm{i}\frac{\omega\tau_2+\phi\left(\omega\right)}{2}\right]+\exp\left[-\mathrm{i}\frac{\omega\tau_2+\phi\left(\omega\right)}{2}\right]\right\},$$

$$\sin\left[\Theta\left(\omega\right)\right]=-\mathrm{i}\beta\left(\omega\right)=-\frac{\mathrm{i}}{2}\left\{\exp\left[\mathrm{i}\frac{\omega\tau_2+\phi\left(\omega\right)}{2}\right]-\exp\left[-\mathrm{i}\frac{\omega\tau_2+\phi\left(\omega\right)}{2}\right]\right\}, \quad (5)$$

$$\Theta\left(\omega\right)=\frac{\omega\tau_2+\phi\left(\omega\right)}{2}.$$

With the state in Eq. (1) and the field operators in Eqs. (2)–(5), we can calculate the detection possibility as

$$\begin{aligned}&\left\langle 0\right|\hat{E}_1^{(+)}\left(t_1\right)\hat{E}_2^{(+)}\left(t_2\right)\hat{E}_3^{(+)}\left(t_3\right)\hat{E}_4^{(+)}\left(t_4\right)\left|\varphi\right\rangle\\ &=-\int \mathrm{d}\omega_1\mathrm{d}\omega_2\mathrm{d}\omega_3\mathrm{d}\omega_4\mathrm{d}\omega_{\mathrm{A}}\mathrm{d}\omega_{\mathrm{B}}\mathrm{d}\omega_{\mathrm{A}}^{'}\mathrm{d}\omega_{\mathrm{B}}^{'}\Phi(\omega_{\mathrm{A}},\omega_{\mathrm{B}})\Phi(\omega_{\mathrm{A}}^{'},\omega_{\mathrm{B}}^{'})\\ &\sin\left[\Theta\left(\omega_1\right)\right]\cos\left[\Theta\left(\omega_2\right)\right]\cos\left[\Theta\left(\omega_3\right)\right]\sin\left[\Theta\left(\omega_4\right)\right]\\ &\exp\left(-\mathrm{i}\omega_1 t_1\right)\exp\left(-\mathrm{i}\omega_2 t_2\right)\exp\left(-\mathrm{i}\omega_3 t_3\right)\exp\left(-\mathrm{i}\omega_4 t_4\right)\\ &\exp\left[-\mathrm{i}\left(\omega_{\mathrm{A}}+\omega_{\mathrm{A}}^{'}\right)\tau_1\right]\left\langle 0\right|\hat{a}_C\left(\omega_1\right)\hat{a}_C\left(\omega_2\right)\hat{a}_D\left(\omega_3\right)\hat{a}_D\left(\omega_4\right)\\ &\hat{a}_{\mathrm{A}}^{\dagger}\left(\omega_{\mathrm{A}}\right)\hat{a}_{\mathrm{A}}^{\dagger}\left(\omega_{\mathrm{A}}^{'}\right)\hat{a}_{\mathrm{B}}^{\dagger}\left(\omega_{\mathrm{B}}\right)\hat{a}_{\mathrm{B}}^{\dagger}\left(\omega_{\mathrm{B}}^{'}\right)\left|0\right\rangle. \end{aligned} \quad (6)$$

At the position of the last BS of the HOM interferometer, the output modes $\hat{a}_C(\omega)$ and $\hat{a}_D(\omega)$ are related to $\hat{a}_{\rm A}(\omega)$ and $\hat{a}_{\rm B}(\omega)$ by

$$\begin{pmatrix}\hat{a}_C(\omega)\\ \hat{a}_D(\omega)\end{pmatrix}=\frac{1}{\sqrt{2}}\begin{pmatrix}1 & 1\\ -1 & 1\end{pmatrix}\begin{pmatrix}\hat{a}_{\rm A}(\omega)\\ \hat{a}_{\rm B}(\omega)\end{pmatrix}. \tag{7}$$

So, the coincidence counting rate can be derived:

$$\begin{aligned}R&=\int \mathrm{d}t_1\mathrm{d}t_2\mathrm{d}t_3\mathrm{d}t_4\left|\left\langle 0\right|\hat{E}_1^{(+)}(t_1)\hat{E}_2^{(+)}(t_2)\hat{E}_3^{(+)}(t_3)\hat{E}_4^{(+)}(t_4)\left|\varphi\right\rangle\right|^2\\ &=\pi^4\int \mathrm{d}\omega_{\rm A}\mathrm{d}\omega_{\rm B}\Phi(\omega_{\rm A},\omega_{\rm B})\Phi(\omega_{\rm A},\omega_{\rm B})\Phi^*(\omega_{\rm A},\omega_{\rm B})\Phi^*(\omega_{\rm A},\omega_{\rm B})\left\{\left[\sin^2\left[\Theta(\omega_{\rm A})\right]\cos^2\left[\Theta(\omega_{\rm B})\right]+\sin^2\left[\Theta(\omega_{\rm B})\right]\cos^2\left[\Theta(\omega_{\rm A})\right]\right]^2\right.\\ &\quad\left.+2\sin^2\left[\Theta(\omega_{\rm A})\right]\cos^2\left[\Theta(\omega_{\rm A})\right]\cos^2\left[\Theta(\omega_{\rm B})\right]\sin^2\left[\Theta(\omega_{\rm B})\right]\right\}+\pi^4\int \mathrm{d}\omega_{\rm A}\mathrm{d}\omega_{\rm B}\Phi(\omega_{\rm A},\omega_{\rm B})\Phi(\omega_{\rm A},\omega_{\rm B})\Phi^*(\omega_{\rm B},\omega_{\rm A})\Phi^*(\omega_{\rm B},\omega_{\rm A})\\ &\quad\left\{\left[\sin^2\left[\Theta(\omega_{\rm A})\right]\cos^2\left[\Theta(\omega_{\rm B})\right]+\sin^2\left[\Theta(\omega_{\rm B})\right]\cos^2\left[\Theta(\omega_{\rm A})\right]\right]^2\right.\\ &\quad\left.+2\sin^2\left[\Theta(\omega_{\rm A})\right]\cos^2\left[\Theta(\omega_{\rm A})\right]\cos^2\left[\Theta(\omega_{\rm B})\right]\sin^2\left[\Theta(\omega_{\rm B})\right]\right\}\exp\left[2\mathrm{i}(\omega_{\rm B}-\omega_{\rm A})\tau_1\right].\end{aligned} \tag{8}$$

The Taylor expansion of the phase shift $\phi(\omega)$[30] which is caused by the dispersive medium when the photons travel through is

$$\begin{aligned}\phi(\omega_j)&=c_0+c_1(\omega_j-\Omega_0)+c_2(\omega_j-\Omega_0)^2\\ &\quad+c_3(\omega_j-\Omega_0)^3+\cdots(j=\mathrm{A},\mathrm{B}),\end{aligned} \tag{9}$$

where C_0 is a constant, C_1 is the first-order dispersion coefficient mainly determined by the inverse of the group velocity, and C_2 is the second-order dispersion coefficient caused by the group velocity dispersion. The third-order dispersion coefficient C_3 mainly contributes to the asymmetry owing to the distortion of the photon wave packets. Higher order dispersion coefficients can be ignored unless we use a strongly dispersive material.

For the assumptions which we declared in the SPDC process, if the central frequency of the down-converted photons is Ω_0, then we have $\omega_{\rm A}=\Omega_0+\omega$ ($\omega_{\rm B}=\Omega_0-\omega$) as the signal (idler) photon frequency. Then the coincidence counting rate can be simplified as

$$\begin{aligned}R&\propto\int \mathrm{d}\omega\left\{\left[f(\omega)f^*(\omega)\right]^2+\left[f(-\omega)f^*(-\omega)\right]^2\right.\\ &\quad\left.+\left[\left[f(\omega)f^*(-\omega)\right]^2\exp(-4\mathrm{i}\omega\tau_1)+C.C.\right]\right\}\\ &\quad\times\left\{22+2\exp\left[2\mathrm{i}\left((\Omega_0+\omega)\tau_2+\phi(\Omega_0+\omega)\right)\right]\right.\\ &\quad+2\exp\left[2\mathrm{i}\left((\Omega_0-\omega)\tau_2+\phi(\Omega_0-\omega)\right)\right]\\ &\quad+3\exp\left[2\mathrm{i}\left(2\Omega_0\tau_2+\phi(\Omega_0+\omega)+\phi(\Omega_0-\omega)\right)\right]\\ &\quad+3\exp\left[2\mathrm{i}\left(2\omega\tau_2+\phi(\Omega_0+\omega)-\phi(\Omega_0-\omega)\right)\right]\\ &\quad-16\exp\left[\mathrm{i}\left(2\Omega_0\tau_2+\phi(\Omega_0+\omega)+\phi(\Omega_0-\omega)\right)\right]\\ &\quad\left.-16\exp\left[\mathrm{i}\left(2\omega\tau_2+\phi(\Omega_0+\omega)-\phi(\Omega_0-\omega)\right)\right]+C.C.\right\}\end{aligned} \tag{10}$$

In order to make Eq. (10) more obvious to get a better understanding, we can rewrite Eq. (10) as a linear superposition

$$R=B+R_0(\tau_1)+R_{\rm even}(\tau_1,\tau_2)+R_{\rm odd}(\tau_1,\tau_2)+R_S(\tau_1,\tau_2). \tag{11}$$

The first term B in Eq. (11) is a constant which corresponds to all terms that are not dependent on the tunable time delay τ_1 after integration, while the second term $R_0(\tau_1)$ is mainly responsible for the central peak around $\tau_1=0$. However, the third one $R_{\rm even}(\tau_1,\tau_2)$ is dependent on the term $\phi(\Omega_0+\omega)+\phi(\Omega_0-\omega)$, thus the odd terms are cancelled and it is sensitive only to the even-order terms. Similarly, the fourth term $R_{\rm odd}$ is dependent on the term $\phi(\Omega_0+\omega)-\phi(\Omega_0-\omega)$, which demonstrates the well-known even-order dispersion cancellation effect. The last term R_S, although contains both the terms $\phi(\Omega_0+\omega)$ and $\phi(\Omega_0-\omega)$ in it, is only a small value after integration. The expansion of each term is shown as

$$\begin{aligned}B&\propto\int \mathrm{d}\omega\left\{\left[f(\omega)f^*(\omega)\right]^2+\left[f(-\omega)f^*(-\omega)\right]^2\right\}\\ &\quad\times\left\{22+2\exp\left[2\mathrm{i}\left((\Omega_0+\omega)\tau_2+\phi(\Omega_0+\omega)\right)\right]\right.\\ &\quad+2\exp\left[2\mathrm{i}\left((\Omega_0-\omega)\tau_2+\phi(\Omega_0-\omega)\right)\right]\\ &\quad+3\exp\left[2\mathrm{i}\left(2\Omega_0\tau_2+\phi(\Omega_0+\omega)+\phi(\Omega_0-\omega)\right)\right]\\ &\quad+3\exp\left[2\mathrm{i}\left(2\omega\tau_2+\phi(\Omega_0+\omega)-\phi(\Omega_0-\omega)\right)\right]\\ &\quad-16\exp\left[\mathrm{i}\left(2\Omega_0\tau_2+\phi(\Omega_0+\omega)+\phi(\Omega_0-\omega)\right)\right]\\ &\quad\left.-16\exp\left[\mathrm{i}\left(2\omega\tau_2+\phi(\Omega_0+\omega)-\phi(\Omega_0-\omega)\right)\right]+C.C.\right\},\end{aligned} \tag{12}$$

$$R_0\propto\int \mathrm{d}\omega\left[f(\omega)f^*(-\omega)\right]^2\exp(-4i\omega\tau_1), \tag{13}$$

$$\begin{aligned}R_{\rm even}&\propto\int \mathrm{d}\omega\left[f(\omega)f^*(-\omega)\right]^2\exp(-4\mathrm{i}\omega\tau_1)\\ &\quad\times\left\{3\exp\left[2\mathrm{i}\left(2\Omega_0\tau_2+\phi(\Omega_0+\omega)+\phi(\Omega_0-\omega)\right)\right]\right.\\ &\quad\left.-16\exp\left[\mathrm{i}\left(2\Omega_0\tau_2+\phi(\Omega_0+\omega)+\phi(\Omega_0-\omega)\right)\right]+C.C.\right\},\end{aligned} \tag{14}$$

$$R_{\text{odd}} \propto \int \mathrm{d}\omega \left[f(\omega) f^{*}(-\omega) \right]^{2} \exp(-4\mathrm{i}\omega\tau_{1}) \times \left\{ 3\exp\left[2\mathrm{i}\left(2\omega\tau_{2} + \phi(\Omega_{0} + \omega) - \phi(\Omega_{0} - \omega) \right) \right] - 16\exp\left[\mathrm{i}\left(2\omega\tau_{2} + \phi(\Omega_{0} + \omega) - \phi(\Omega_{0} - \omega) \right) \right] + C.C. \right\}, \quad (15)$$

$$R_{\text{S}} \propto \int \mathrm{d}\omega \left[f(\omega) f^{*}(-\omega) \right]^{2} \exp(-4\mathrm{i}\omega\tau_{1}) \times \left\{ \exp\left[2\mathrm{i}\left((\Omega_{0} + \omega)\tau_{2} + \phi(\Omega_{0} + \omega) \right) \right] + \exp\left[2\mathrm{i}\left((\Omega_{0} - \omega)\tau_{2} + \phi(\Omega_{0} - \omega) \right) + C.C. \right] \right\}. \quad (16)$$

Our results are illustrated by a numerical simulation with feasible experimental parameters. We use a continuous pump laser with central frequency of 406 nm to pump a type-II degenerate BBO crystal. We choose strong dispersive media for the phase shift and the fixed time delay we set is $\tau_2 = 26$ ps, which is much greater than the coherence time of the photons.

From Figs. 3(a) and (b), we can observe more intuitively what we have discussed above. The terms R_0 and R_{even} are responsible for the central peak of the coincidence counting rate R, in which R_{even} demonstrates the odd-order dispersion cancellation effect. In Fig. 3(c), R_{odd} with four side fringes demonstrates the even-order dispersion cancelation effect. The term R_{s}, which is shown in Fig. 3(d), mainly contributes to the even-order dispersion cancellation around $\tau_1 = \pm 26$ ps compared with Fig. 3(c).

Let us take into account the condition that each MZ interferometer is fed with photons composed of a signal photon and an idler photon as a pair no matter which region we scan the time delay τ_1 into. Although in this case, the two detectors after each MZ interferometer do not fire at the same time, we cannot yet distinguish which signal (idler) photon is sent into the upper (lower) arm of the MZ interferometer. Furthermore, if the two signal (idler) photons are sent into the MZ interferometer together as a pair, and the pairs all follow the same long (short) path, interference can also occur because the detectors can fire at the same time. So small oscillation fringes which are caused by interference can exist at all times. These belong to the indistinguishability of two photons.

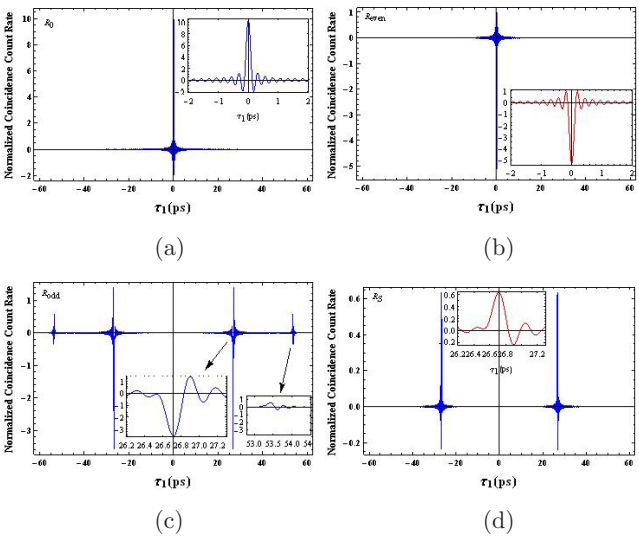

Fig. 3. Coincidence counting rate of (a) R_0 is the main central peak of the total coincidence counting rate and (b) R_{even} is caused by the odd-order dispersion cancellation shown in the region of $\tau_1 \approx 0$ ps, (c) R_{odd}, four asymmetric fringes are shown in the region of $\tau_1 \approx \pm 26$ and ± 52 ps, which are caused by the even-order dispersion cancellation, and (d) R_{s} mainly contributes to the even-order dispersion cancellation around ($\tau_1 \approx \pm 26$ ps,).

In Fig. 2, when we scan into the region around $\tau_1 \approx 0$ ps, we can observe a maximum peak. It is because in this stage, the four photons can arrive at the last BS of the HOM interferometer simultaneously, so we cannot tell which two photons enter into each MZ interferometer. This belongs to the indistinguishability of four photons. Besides, there are also two kinds of events that we cannot distinguish: 1) whether two photons which enter into each MZ interferometer both traverse along the long path or the short one and 2) whether photons which arrive at the last BS of each MZ interferometer are reflected or transmitted. This time it belongs to the indistinguishability of two photons.

As we continue to scan the time delay in the region of $\tau_1 \approx \pm 26$ ps, we can consider the case that each MZ interferometer has a signal and an idler photon to enter into as a pair, with the signal photons which had already been delayed by about ±26 ps following the short path, whereas the idler following the long one in the MZ interferometer. In this case, the four detectors can fire at the same time, but we cannot distinguish which signal (idler) photons enter into the upper (lower) MZ interferometer. Moreover, whether the photons are reflected or transmitted on the last BS of each MZ interferometer cannot be distinguished either. Thus interference can occur at this stage.

Lastly, when it reaches into the region of $\tau_1 \sim \pm 52$ ps, despite the cases which we have discussed about in the general cases, there are two indistinguishable events

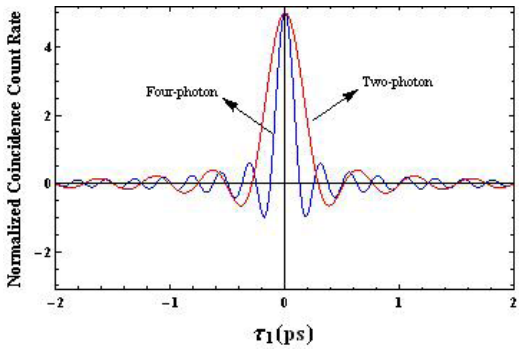

Fig. 4. Comparison of the central peak of the coincidence counting rate between the two-photon project and the four-photon one. The red curve represents the two-photon case, whereas the blue one represents the four-photon situation.

that the two detectors fire with a time interval of 26 ps taking place: 1) each MZ interferometer is fed with a signal photon and an idler photon as a pair, the signal photons follow the short path, whereas the idler photons follow the long one and 2) the two photons which enter into each MZ interferometer are both the signal (idler) photons. And in these events, we cannot tell which two photons enter into each MZ interferometer. Thus, this indistinguishability can lead to interference with a small possibility.

From the above discussion, we get a better understanding of the interference effect happened in the four-photon interferometer through the phenomena that even- and odd-order dispersion cancellation can show up in different regions when we modulate the time delay continuously.

Then we compare our four-photon scheme with the two-photon which has only one MZ interferometer in one of the HOM interferometer outputs. We find that in our scheme the full-width at half-maximum of the central peak is about 1/2 narrower than the two-photon case (Fig. 4). It is known that in quantum optics, an ensemble of photons is treated as a Bose condensate with a de Broglie wavelength given by λ_0/N[31], which has already been experimentally confirmed[32,33], where λ_0 is the wavelength and N is the average number of photons. This is an implication of the phase shift $N\Delta\varphi$ of the four photons which is induced by the path length, where $\Delta\varphi$ is the phase modulation of a single photon. Thus, the four-photon scheme gets a better resolution than the two-photon one.

In conclusion, we theoretically demonstrate a dispersion cancellation scheme based on the four-photon quantum interference. The interesting thing of the scheme is that it can not only show the even- and odd-order dispersion cancellation effects, which can help to get a better understanding of the interference effects shown in the four-photon system; but also get a much narrower width of the interference fringes, from which we can get a better resolution than the state-of-the-art two-photon interferometry. Although there is actual limitation due to the low coincidence count rates, it can eventually overcome with the next generation of entangled photon sources and detectors. It is expected that the scheme can extend the application of multi-photon system such as in quantum metrology.

This work was supported by the National Natural Science Foundation of China under Grant Nos. 61275122, 11105205, and 61222504.

References

1. V. Giovannetti, S. Lloyd, L. Maccone and F. N. C. Wong, J. Opt. B: Quant. Semiclass Opt. **4,** S415 (2001).
2 A. Manita, Queue. Syst. **76,** 149 (2014).
3. Y. L. Zhang, Y. R. Zhang, L. Z. Mu, and H. Fan, Phys. Rev. A **88,** 052314 (2013).
4. A. Grebenyuk, A. Federici, V. Ryabukho, and A. Dubois, Appl. Opt. **53,** 1697 (2014).
5. M. D. Mazurek, K. M. Schreiter, R. Prevedel, R. Kaltenbaek, and K. J. Resch, Sci. Rep. **3,** 1582 (2013).
6. A. Zhang, M. Li, and Y. Feng, Chin. Opt. Lett. **11,** 092701 (2013).
7. A. M. Steinberg, P. G. Kwiat, and R. Y. Chiao, Phys. Rev. A **45,** 6659 (1992).
8. M. Okano, R. Okamoto, A. Tanaka, S. Ishida, N. Nishizawa, and S. Takeuchi, Phys. Rev. A **88,** 043845 (2013).
9. J. D. Franson, Phys. Rev. A **45,** 3126 (1992).
10. J. D. Franson, Phys. Rev. A **80,** 032119 (2009).
11. K. A. O'Donnell, Phys. Rev. Lett. **106,** 063601 (2011).
12. M. B. Nasr, S. Carrasco, B. E. A. Saleh, A. V. Sergienko, M. C. Teich, J. P. Torres, L. Torner, D. S. Hum, and M. M. Fejer, Phys. Rev. Lett. **100,** 183601 (2008).
13. S. Y. Baek, Y. W. Cho, and Y. H. Kim, Opt. Express **17,** 19241 (2009).
14. T. Zhong and F. N. C. Wong, Phys. Rev. A **88,** 020103 (2013).
15. O. Minaeva, C. Bonato, B. E. A. Saleh, D. S. Simon, and A. V. Sergienko, Phys. Rev. Lett. **102,** 100504 (2009).
16. M. Yabuno, R. Shimizu, Y. Mitsumori, H. Kosaka, and K. Edamatsu, Phys. Rev. A **86,** 010302(R) (2012).
17. Y. F. Huang, B. H. Liu, L. Peng, Y. H. Li, L. Li, C. F. Li, and G. C. Guo, Nat. Commun. **2,** 546 (2011).
18. X. C. Yao, T. X. Wang, P. Xu, H. Lu, G. S. Pan, X. H. Bao, C. Z. Peng, C. Y. Lu, Y. A. Chen, and J. W. Pan, Nat. Photon. **6,** 225 (2012).
19. B. H. Liu, F. W. Sun, Y. X. Gong, Y. F. Huang, G. C. Guo, and Z. Y. Ou, Opt. Lett. **32,** 1320 (2007).
20. X. L. Niu, Y. X. Gong, B. H. Liu, Y. F. Huang, G. C. Guo, and Z. Y. Ou, Opt. Lett. **34,** 1297 (2009).
21. R. Birrittella, J. Mimih, and C. C. Gerry, Phys. Rev. A **86,** 063828 (2012).
22. R. Krischek, C. Schwemmer, W. Wieczorek, H. Weinfurter, P. Hyllus, L. Pezzé, and A. Smerzi, Phys. Rev. Lett. **107,** 080504 (2011).
23. B. Liu and Z. Y. Ou, Phys. Rev. A **81,** 023823 (2010).
24. Z. Y. Ou, Phys. Rev. A **55,** 2598 (1997).
25. F. W. Sun, B. H. Liu, Y. F. Huang, Z. Y. Ou, and G. C. Guo, Phys. Rev. A **74,** 033812 (2006).
26. B. H. Liu, F. W. Sun, Y. X. Gong, Y. F. Huang, Z. Y. Ou, and G. C. Guo, Phys. Rev. A **77,** 023815 (2008).
27. D. W. Berry, M. J. W. Hall, and H. M. Wiseman, Phys. Rev. Lett. **111,** 113601 (2013).
28. P. Walther, J. W. Pan, M. Aspelmeyer, R. Ursin, S. Gasparoni, and A. Zeilinger, Nature **429,** 158 (2004).
29. X. Fan, Y. Huang, X. Ren, X. Duan, F. Hu, and Q. Wang, Chin. Opt. Lett. **10,** 110402 (2012).
30. J. C. Diels and W. Rudolph, *Ultrashort Laser Pulse Phenomena* (Elsevier Inc. Academic Press, 2006).
31. J. Jacobson, G. Bjork, I. Chuang, and Y. Yamamoto, Phys. Rev. Lett. **74,** 4835 (1995).
32. T. Nagata, R. Okamoto, J. L. O'Brien, K. Sasaki, and S. Takeuchi, Science **316,** 726 (2007).